



Reax Engineering Inc.
1958 University Ave, Suite B
Berkeley, CA 94704

Job # 12-0222


High Resolution Wind Loading Study

Prepared for Southern California Edison
Three Innovation Way
Pomona, CA 91768

SCE Purchase Order Number 4500546849

Proprietary and Confidential

Revision 0 – March 26, 2013

	Prepared by	Reviewed by	Professional Engineer Seal
Name	Chris Lautenberger, PhD, PE		
Signature			

DISCLAIMER

THIS DOCUMENT AND THE MODEL/DATA DESCRIBED HEREIN ARE PROVIDED ON AN “AS IS” BASIS. GIVEN THE COMPLEXITY AND THE NUMBER OF RELEVANT VARIABLES, WIND LOADS CANNOT BE PREDICTED OR ASSESSED WITH COMPLETE ACCURACY. ACCORDINGLY, REAX ENGINEERING INC., ITS SUPPLIERS, AND LICENSORS, TO THE FULLEST EXTENT PERMITTED BY LAW, DISCLAIM ALL WARRANTIES, EITHER EXPRESS OR IMPLIED, STATUTORY OR OTHERWISE, INCLUDING BUT NOT LIMITED TO THE IMPLIED WARRANTIES OF MERCHANTABILITY AND FITNESS FOR PARTICULAR PURPOSE WITH RESPECT TO THE MODELING AND DATA DESCRIBED HEREIN. IN NO EVENT SHALL REAX ENGINEERING INC., ITS SUPPLIERS, OR LICENSORS BE LIABLE FOR ANY DAMAGES (INCLUDING, WITHOUT LIMITATION, INCIDENTAL AND CONSEQUENTIAL DAMAGES, LOST PROFITS, OR DAMAGES RESULTING FROM BUSINESS INTERRUPTION OR PERSONAL INJURY/WRONGFUL DEATH) ARISING OUT OF THE USE OF THIS WORK, WHETHER BASED ON WARRANTY, CONTRACT, TORT, OR ANY OTHER LEGAL THEORY, AND WHETHER OR NOT REAX ENGINEERING INC. IS ADVISED OF THE POSSIBILITY OF SUCH DAMAGES.

High Resolution Wind Loading Study
Proprietary and Confidential

Document Revision History



Job #	Job Name	Client
12-0222	High Resolution Wind Loading Study	Southern California Edison

Report title: High Resolution Wind Loading Study Methodology

Revision #	Date	Description	
Rev 0	March 26, 2013	Initial draft.	
		Prepared by: Chris Lautenberger, PhD, PE	Reviewed by:
		Prepared by:	Reviewed by:
		Prepared by:	Reviewed by:
		Prepared by:	Reviewed by:
		Prepared by:	Reviewed by:

High Resolution Wind Loading Study
Proprietary and Confidential

TABLE OF CONTENTS

1.0	INTRODUCTION	1
2.0	IDENTIFICATION OF HISTORICAL WIND AND FIRE WEATHER EVENTS	2
2.1	HIGH WINDS WITHOUT CONSIDERATION OF RELATIVE HUMIDITY AND TEMPERATURE	2
2.2	HIGH WINDS OCCURRING SIMULTANEOUSLY WITH LOW RELATIVE HUMIDITY AND HIGH TEMPERATURES	4
3.0	RECONSTRUCTION OF HISTORICAL WIND EVENTS USING HIGH RESOLUTION NUMERICAL WEATHER PREDICTION	7
4.0	RESULTS.....	11
4.1	HIGH WINDS WITHOUT CONSIDERATION OF RELATIVE HUMIDITY AND TEMPERATURE	11
4.2	HIGH WINDS OCCURRING SIMULTANEOUSLY WITH LOW RELATIVE HUMIDITY AND HIGH TEMPERATURES	12
5.0	VALIDATION OF NUMERICAL WEATHER PREDICTION WITH WEATHER STATION DATA 13	
6.0	REFERENCES	15

High Resolution Wind Loading Study
Proprietary and Confidential

LIST OF FIGURES

FIGURE 1. CURRENT WRF NESTS. RED AREA IS SCE SERVICE TERRITORY	7
FIGURE 2. THE DURST CURVE - RATIO OF MAXIMUM WIND SPEED OVER T SECONDS TO HOURLY MEAN WIND SPEED (ASCE 7-10 FIGURE C26.5-1).	10
FIGURE 3. COMPOSITE WIND LOADING MAP FOR PEAK WIND SPEEDS WITHOUT CONSIDERATION OF RELATIVE HUMIDITY AND TEMPERATURE. VELOCITIES ARE 20 FT WIND SPEEDS (3 SECOND GUSTS) FOR A 50-YEAR RETURN INTERVAL.	11
FIGURE 4. COMPOSITE WIND LOADING MAP FOR PEAK WIND SPEEDS OCCURRING SIMULTANEOUSLY WITH LOW RELATIVE HUMIDITY AND HIGH TEMPERATURES. VELOCITIES ARE 20 FT WIND SPEEDS (3 SECOND GUSTS) FOR A 50-YEAR RETURN INTERVAL.	12
FIGURE 5. EXAMPLE OF COMPARISON BETWEEN SIMULATED (WRF) WIND SPEED/DIRECTION, AIR TEMPERATURE, AND RELATIVE HUMIDITY WITH SURFACE INTEGRATED SURFACE DATABASE (ISD) DATA.	14

High Resolution Wind Loading Study
Proprietary and Confidential

LIST OF TABLES

TABLE 1. HISTORICAL HIGH WIND EVENTS IN SCE’S SERVICE TERRITORY IDENTIFIED USING NARR DATA FROM 1979-2012. RANKING CRITERION IS WIND SPEED ONLY (NO CONSIDERATION OF TEMPERATURE AND HUMIDITY).....	3
TABLE 2. IGNITION PROBABILITY BY WOODY EMBERS/FIREBRANDS AS TABULATED BY SCHROEDER [3].	5
TABLE 3. HISTORICAL HIGH WIND / LOW RELATIVE HUMIDITY / HIGH TEMPERATURE EVENTS IN SCE’S SERVICE TERRITORY IDENTIFIED USING NARR DATA FROM 1979-2012. RANKING CRITERION IS MODIFIED FOSBERG FIRE WEATHER INDEX (SIMULTANEOUSLY CONSIDERS WIND SPEED, RELATIVE HUMIDITY, AND TEMPERATURE).....	6
TABLE 4. RATIO OF T-YEAR RETURN INTERVAL WIND SPEED TO 34-YEAR RETURN INTERVAL WIND SPEED.	9

1.0 INTRODUCTION

Reax Engineering Inc. (Berkeley, CA) has been contracted by Southern California Edison (SCE) to conduct a high-resolution wind-loading analysis across its service territory¹. The primary project deliverable is a series of Geographic Information System (GIS) based high resolution wind loading maps across SCE's service territory. These maps have been provided to SCE in electronic format. This report documents the methodology that was applied to develop these maps.

Weather stations in California are too sparsely spaced to be useful for characterizing spatial wind patterns and developing wind loads. Therefore, a general-purpose mesoscale numerical weather prediction (NWP) model, Weather Research and Forecasting (WRF) [1], was used to characterize wind loads across SCE's service territory during actual wind events that have occurred since 1979. To the extent possible, this work has been conducted under the guidance of relevant sections of ASCE/SEI 7-10 "Minimum Design Loads for Buildings and Other Structures" and California General Order 95 "Overhead Electric Line Construction".

¹ SCE Purchase Order Number 4500546849

2.0 IDENTIFICATION OF HISTORICAL WIND AND FIRE WEATHER EVENTS

The first step in the analysis is identification of historical wind and fire weather events to be simulated using high-resolution numerical weather prediction. This was accomplished by analyzing the North American Regional Reanalysis (NARR) dataset to identify historical wind events occurring between 1979 and 2012. The NARR dataset is maintained by the National Centers for Environmental Prediction, the National Weather Service, and the National Oceanic and Atmospheric Administration. It contains gridded meteorological fields at a resolution of 32 km, updated every 3 hours, from 1 January 1979 through present day. The NARR dataset is based on a combination of historical observations and weather modeling; it is the standard dataset used for analyses of historical weather in the US. The primary advantage of identifying historical wind events using reanalysis data, instead of surface (weather station) observations, is that the NARR dataset is both spatially and temporally uniform whereas point observation data are not.

Historical wind and fire weather events in SCE's service territory were identified by developing a script to extract wind, temperature, and humidity data from the GRIdded Binary (GRIB) NARR data and convert it to compressed GeoTIFF format, clipping away areas outside of SCE's service territory. Next, computer programs were developed to process this NARR data and systematically identify dates where high winds or severe fire weather were encountered. Separate dates were used for wind events and fire weather events. The procedure that was used to identify high wind events, without consideration of relative humidity and temperature, is described in Section 2.1. Similarly, the procedure used to identify fire weather events (i.e., high winds that occurred simultaneously with low humidity and high temperature) is described in Section 2.2.

2.1 High winds without consideration of relative humidity and temperature

A spatial filter was applied to the NARR dataset to determine the maximum wind speed experienced at any point in SCE's service territory at a particular date and time. This filter was then used to identify the 34 most severe wind events (because 34 years of data were analyzed) between 1979 and 2012. The historical wind events identified using this filter are shown in Table 1. Note that this spatial filtering approach treats all areas in SCE's service territory equally, even if limited population and/or overhead electrical facilities are present.

It is seen that most of the dates identified in Table 1 fall between December and March. Winter wind events in California are usually associated with lower temperatures and higher relative humidities compared to wind events occurring from early summer through late fall. The wind speeds listed in Table 1 are wind speeds from the NARR dataset and are expected to be considerably lower than gust wind speeds measured at weather stations.

High Resolution Wind Loading Study
Proprietary and Confidential

Table 1. Historical high wind events in SCE's service territory identified using NARR data from 1979-2012. Ranking criterion is wind speed only (no consideration of temperature and humidity).

#	Date (UTC)	Maximum wind speed (mph)	Average wind speed (mph)
1	12/12/1995	51.5	17.3
2	12/31/2005	49.1	18.4
3	12/16/1987	47.6	16.1
4	1/4/2008	47.0	19.1
5	2/6/1998	46.0	19.2
6	12/1/2011	45.8	21.2
7	2/18/1993	45.1	15.1
8	11/24/2001	44.3	17.3
9	12/1/2005	44.2	13.5
10	10/25/2010	44.0	16.9
11	1/12/1980	43.8	13.0
12	12/19/2010	43.4	18.4
13	2/17/1986	43.2	12.7
14	11/14/1981	42.5	12.5
15	1/9/2005	42.3	14.9
16	1/24/1983	42.2	13.4
17	2/4/1989	41.8	16.9
18	1/18/1988	41.7	16.4
19	1/2/2006	41.7	22.1
20	12/25/2008	41.7	20.1
21	10/14/2009	41.5	16.7
22	3/8/1986	41.2	14.9
23	12/8/1988	41.1	16.6
24	12/19/1990	41.1	20.1
25	3/27/1985	40.9	18.9
26	12/11/1997	40.8	15.1
27	2/8/1985	40.8	11.8
28	2/14/2000	40.7	14.07
29	1/1/1997	40.7	9.94
30	1/6/2007	40.6	13.83
31	2/3/2008	40.6	20.87
32	3/3/1991	40.4	12.04
33	1/6/2003	40.3	16.52
34	11/20/2009	40.1	11.89

2.2 High winds occurring simultaneously with low relative humidity and high temperatures

A second spatial filter is used to identify high wind events that occur simultaneously with high temperature and low relative humidity. This spatial filter is a combination of the Fosberg Fire Weather Index (FFWI) [2] and Schroeder ember ignition probability [3].

The Fosberg Fire Weather Index combines temperature, relative humidity, and wind speed into a single index as follows:

$$FFWI = \eta \sqrt{1 + U^2} \quad (1)$$

where U is the 20-ft wind speed in miles per hour and η is a function of equilibrium moisture content, M_{eq} :

$$\eta = 1 - 2\left(\frac{M_{eq}}{30}\right) + 1.5\left(\frac{M_{eq}}{30}\right)^2 - 0.5\left(\frac{M_{eq}}{30}\right)^3 \quad (2)$$

In Equation 2, M_{eq} is calculated as [4, 5]:

$$M_{eq} = \begin{cases} 0.03 + 0.28 \times RH - 0.00058 \times RH \times T & \text{for } RH < 10\% \\ 2.23 + 0.16 \times RH - 0.0148 \times T & \text{for } 10 \leq RH < 50\% \\ 21.1 - 0.4944 \times RH + 0.00557 \times RH^2 - 0.00035 \times RH \times T & \text{for } RH \geq 50\% \end{cases} \quad (3)$$

where RH is relative humidity in percent and T is temperature in °F.

FFWI is very sensitive to wind speed, and less sensitive to fuel moisture content. For example, FFWI is 80 for a wind speed of 50 mph and an equilibrium moisture content of 10%, but only 73 for a wind speed of 25 mph and an equilibrium moisture content of 2%. Ignition and growth of a wildland fire to threatening scales is more likely under the latter conditions, but spread rates for an *already established* wildland fire could be higher under the former conditions. For this reason, a Modified Fosberg Fire Weather Index (MFFWI) is used in this work to identify wind events that occur simultaneously with low relative humidities and high temperatures. MFFWI is defined as follows:

$$MFFWI = FFWI \times \frac{P_{ign}}{100} \quad (4)$$

where P_{ign} is Schroeder's ember ignition probability as calculated with Equation 5 below. Schroeder's firebrand ignition probabilities are given in Table 2 as a function of fuel temperature and fine fuel moisture content. The data were originally published [3] with temperatures in degrees Fahrenheit and this convention is retained here. It is seen that the ember ignition probability is strongly sensitive to moisture content, and slightly less sensitive to temperature.

High Resolution Wind Loading Study
Proprietary and Confidential

Table 2. Ignition probability by woody embers/firebrands as tabulated by Schroeder [3].

<i>Fuel</i>	<i>Fine Fuel Moisture Content (%)</i>														
<i>Temp (F)</i>	1.5	2.0	2.5	3.0	4.0	5.0	6.0	7-8	9-10	11-12	13-16	17-20	21-25	26-30	>30
30-39	87	80	74	69	59	51	43	34	25	17	10	4	1	0	0
40-49	89	83	77	71	61	53	45	36	26	18	11	5	1	0	0
50-59	92	85	79	73	63	54	47	37	27	20	11	5	2	0	0
60-69	94	88	81	76	65	56	49	39	29	21	12	6	2	0	0
70-79	97	90	84	78	68	59	51	41	30	22	13	6	2	0	0
80-89	100	93	87	81	70	61	53	42	31	23	14	7	2	1	0
90-99	100	96	90	84	73	63	55	44	33	24	15	7	3	1	0
100-109	100	99	93	86	75	66	57	46	35	26	16	8	3	1	0
110-119	100	100	96	89	78	68	59	48	36	27	17	9	3	1	0
120-129	100	100	99	93	81	71	62	51	38	29	18	9	4	1	0
130-139	100	100	100	96	84	74	65	53	40	30	20	10	4	1	0
140-149	100	100	100	99	87	77	67	55	42	32	21	11	5	2	0
150-159	100	100	100	100	90	80	70	58	45	34	22	12	5	2	0

For moisture contents (MC) less than ~10% and fuel bed temperatures (T) between 65 °F and 155 °F, the data in Table 2 are well fit by the following expression:

$$P_{ign} = \min(f_1(MC)f_2(T), 100) \quad (5a)$$

$$f_1(MC) = \frac{107}{1 + 0.028M_{eq}^{1.94}} \quad (5b)$$

$$f_2(T) = 0.677 + 0.00322T \quad (5c)$$

Equation 5 is a curve fit to the data in Table 2 where P_{ign} is the probability that a woody ember could ignite a fuel bed (percent), M_{eq} is equilibrium moisture content (percent) calculated with Equation 3, and T is fuel bed temperature (°F).

Modified Fosberg Fire Weather Index was calculated from the NARR dataset and a spatial filter was applied to the NARR dataset to determine the maximum MFFWI experienced at any point in SCE's service territory at a particular date and time. This filter was then used to identify the 34 most severe fire weather events, using MFFWI as a metric, between 1979 and 2012 (34 years). The historical fire weather events identified using this filter are shown in Table 3. As with the "wind only" filter, this spatial filtering approach treats all areas in SCE's service territory equally, even if limited population and/or overhead electrical facilities are present.

Table 3. Historical high wind / low relative humidity / high temperature events in SCE's service territory identified using NARR data from 1979-2012. Ranking criterion is Modified Fosberg Fire Weather Index (simultaneously considers wind speed, relative humidity, and temperature).

#	Date (UTC)	Maximum MFFWI	Average MFFWI
1	9/15/2006	75.60	30.97
2	8/28/2010	73.48	34.90
3	10/27/2009	70.88	26.44
4	10/22/2007	70.82	22.82
5	8/7/2006	69.68	23.93
6	9/29/2009	68.82	35.62
7	10/25/2003	68.32	29.16
8	8/30/2009	67.89	30.26
9	11/28/2007	67.85	21.08
10	8/6/2009	65.58	28.43
11	8/19/1993	64.98	24.30
12	9/2/2004	64.81	33.54
13	11/3/1990	64.34	21.11
14	10/27/1993	63.89	23.94
15	8/31/2011	63.76	26.65
16	10/11/2008	63.14	24.75
17	10/26/2006	62.96	18.52
18	9/18/2004	62.93	26.03
19	11/7/2002	62.88	20.07
20	8/8/1994	62.60	27.19
21	10/8/2005	61.58	23.74
22	9/28/1999	61.43	22.63
23	9/2/1994	61.43	29.11
24	9/6/1989	61.30	29.35
25	8/28/2002	61.19	23.89
26	10/17/1999	60.90	25.73
27	8/6/2010	60.41	25.53
28	10/5/1993	60.11	18.90
29	10/5/1995	60.03	22.95
30	8/30/1999	59.99	25.99
31	10/26/1980	59.96	17.50
32	10/22/1995	59.96	22.86
33	11/25/1990	59.92	15.96
34	8/6/2007	59.86	23.61

3.0 RECONSTRUCTION OF HISTORICAL WIND EVENTS USING HIGH RESOLUTION NUMERICAL WEATHER PREDICTION

Weather Research and Forecasting (WRF) Version 3.4 was used to reconstruct wind fields at high resolution across SCE's service territory for the high wind / fire weather events identified in Sections 2.1 and 2.2. For each of these events, the NARR dataset described earlier is used to initialize the corresponding WRF simulation and provide lateral boundary conditions.

A telescoping (nested) grid arrangement is used, with the resolution of the coarsest mesh (domain 1) specified as 10.8 km. Two nests, each with a mesh size ratio of 3:1 as is common practice with WRF, are used to provide greater resolution over SCE's service territory. Domain 2 has a resolution of 3.6 km, and domain 3 has a resolution of 1.2 km. Figure 1 shows the extents of the finest two meshes (the outermost/coarsest mesh is not shown) with SCE's service territory shaded in red.

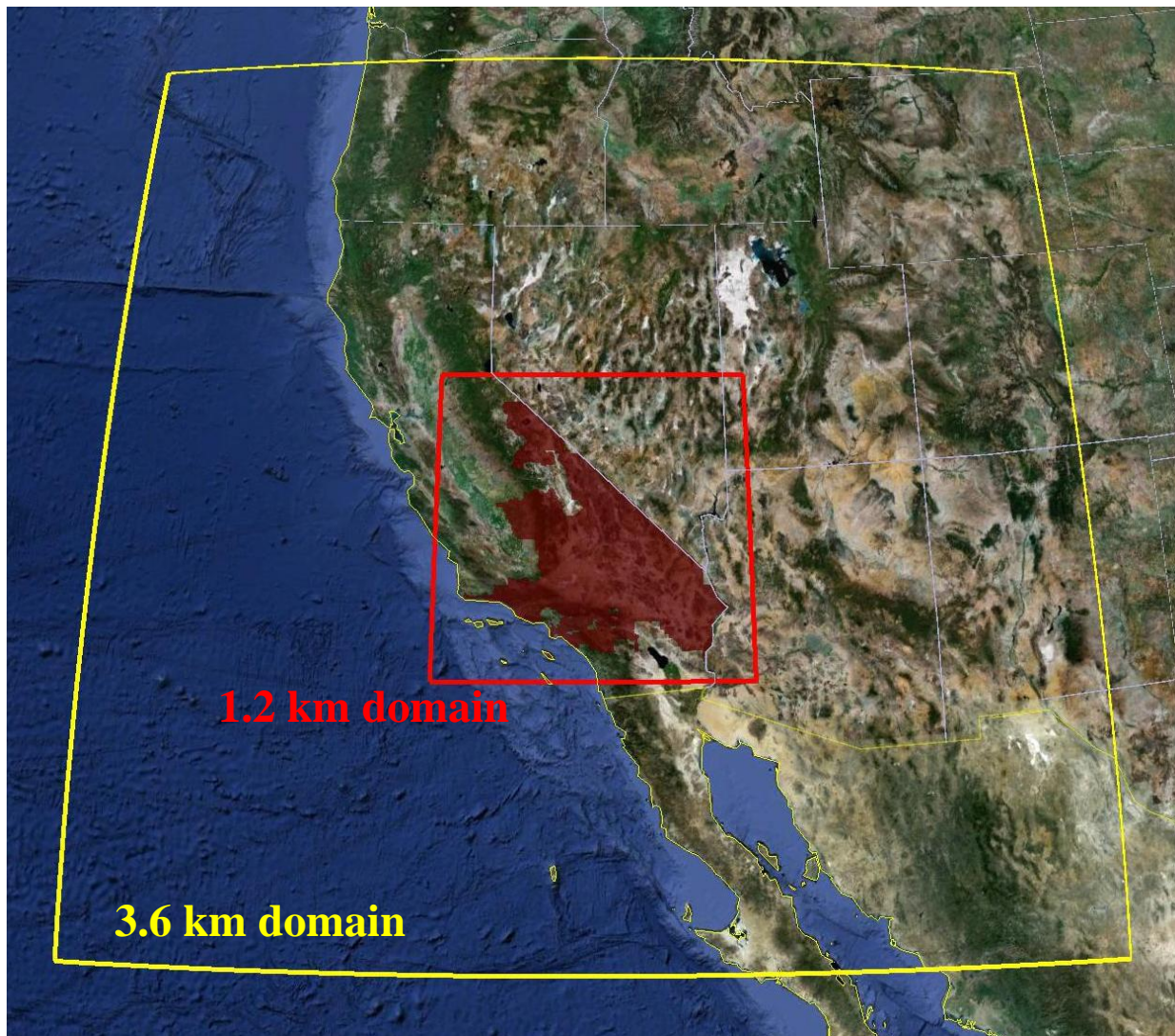


Figure 1. Current WRF nests. Red area is SCE service territory.

Simulations were conducted with a 24-hour “spin up” to allow coherent structures to fully develop within the simulation before the wind event of interest occurs. All meteorological fields generated by WRF have been archived.

The WRF runs were set up to write Network Common Data Form (NetCDF) gridded meteorological fields to disk at an interval of one hour. These hourly NetCDF files were post-processed using ARWpost (Advanced Research WRF postprocessor) and GrADS (Grid Analysis and Display System) to extract hourly fields of wind speed and direction at a height of 10 m as well as temperature and relative humidity at a height of 2 m. Individual hourly rasters were collated into multiband (stacked) GeoTIFF rasters using GDAL (Geospatial Data Abstraction Library). These multiband rasters were then post-processed using custom-developed software to determine, for each wind event identified in Table 1, the peak wind speed occurring at each pixel and, for each fire weather event identified in Table 3, the peak Modified Fosberg Fire Weather Index occurring at each pixel within a 24-hour interval. This process was used to distill, for each event, hourly fields of wind speed/direction and temperature/humidity to a single “event peak” value for each pixel.

Next the 34 “event peak” values were sorted for each pixel to determine the “overall peak” value of wind speed for the events in Table 1 or MFFWI for the events in Table 3. This overall peak value corresponds to the maximum wind speed (for the wind only simulations) or MFFWI (for the fire weather simulations) that occurred over 34 events. Although wind-speed is used as the ranker for the events shown in Table 1 and MFFWI is used as the ranker for the events shown in Table 3, the wind speed associated with the peak MFFWI at each pixel was extracted and used in all additional analysis.

Next, these overall peak values of wind speed are translated to return intervals. Return interval (sometimes called return period or recurrence interval) is defined as follows:

$$\text{return interval} = \frac{n}{m} = T \quad (6)$$

where n is the number of years in the record, and m is the number of recorded occurrences of the event being considered. In this case, $n = 34$ years. Since the overall peak value (of wind speed or MFFWI) has been determined for each pixel, $m = 1$. Consequently, from Equation 6 that the overall peak values correspond, approximately, to a 34-year return interval event.

ASCE 7-10 Equation C26.5-2 can be used to translate the wind speed for any return period to the 50 year return period wind speed as follows:

$$\frac{V_T}{V_{50}} = 0.36 + 0.1 \ln(12T) \quad (7)$$

where T is the return period in years, V_{50} is the 50-year return interval wind speed, and V_T is the T -year return interval wind speed. Substituting $T = 34$ years into Equation 7 gives $V_{34}/V_{50} =$

0.961. This can in turn be used to calculate the ratio of the T -year return interval wind speed to the 34 year return interval wind speed as follows:

$$\frac{V_T}{V_{34}} = \frac{V_{50}}{V_{34}} \frac{V_T}{V_{50}} = \frac{1}{0.961} (0.36 + 0.1 \ln(12T)) = 0.3746 + 0.104 \ln(12T) \quad (8)$$

V_T / V_{34} calculated with Equation 8 for several return intervals is show in Table 4.

Table 4. Ratio of T-year return interval wind speed to 34-year return interval wind speed.

T (years)	V_T / V_{34} (-)
1	0.633
5	0.800
10	0.872
20	0.945
30	0.987
40	1.017
50	1.040
75	1.082
100	1.112

At a resolution of 1.2 km (i.e., the resolution of the finest WRF domain), the wind speeds calculated by WRF approximately to 20 minute averages. However, wind loads are usually given in terms of a 3 second gust. ASCE 7-10 Figure C26.5-1 (the “Durst curve”), repeated below as Figure 2, can be used to convert a wind speed averaged over a particular interval to another interval such as a 3 second gust. From Figure 2, $V_3/V_{3600} \approx 1.53$ (meaning the 3 second gust is 1.53 times the hourly mean wind speed). Similarly, $V_{1200}/V_{3600} \approx 1.04$ (i.e., the 20 minute wind speed is approximately 1.04 times the hourly mean wind speed). Thus, the ratio of the 3 second gust wind speed to the 20 minute (i.e., WRF) wind speed is:

$$\frac{V_3}{V_{1200}} = \frac{V_3}{V_{3600}} \frac{V_{3600}}{V_{1200}} = \frac{1.53}{1.04} = 1.47 \quad (9)$$

For this reason, wind speeds output by WRF are multiplied by this conversion factor (1.47) to determine 3-second gust wind speeds.

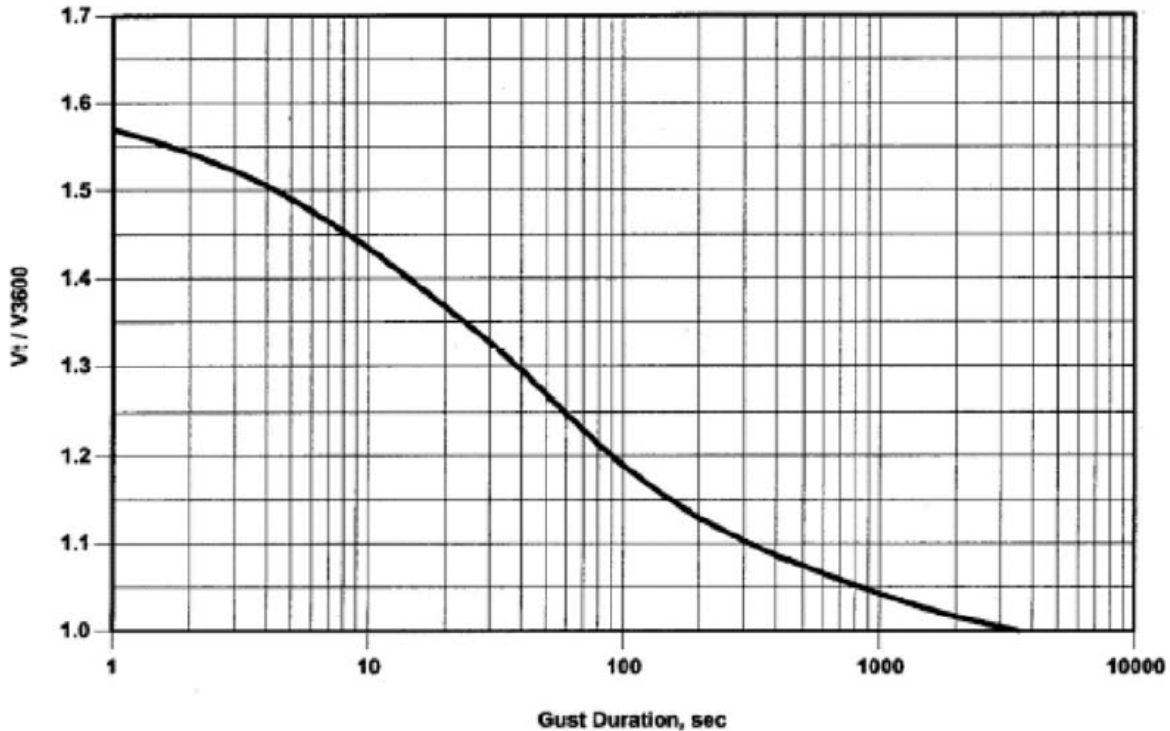


Figure 2. The Durst Curve - ratio of maximum wind speed over t seconds to hourly mean wind speed (ASCE 7-10 Figure C26.5-1).

The wind speeds calculated by WRF is output at a height of 10 m (32.8 ft). In the US, wind speeds are normally reported at a height of 20 ft (6.1 m). The ratio of the 20 ft wind speed to the 10 m wind speed depends on several factors such as surface roughness, but for simplicity it is assumed here that this ratio is constant at 0.87.

Equation 10 summarizes the conversion of the 10 m WRF wind speed in units of m/s to the 20 ft 3 second gust wind speed in units of mph. The factor 2.24 converts m/s to mph; 0.87 converts 10 m wind speed to 20 ft wind speed; and 1.45 converts ~20 minute wind speed to 3 s gust.

$$20 \text{ ft 3-s gust wind speed (mph)} = 10 \text{ m WRF wind speed (m/s)} \times 2.24 \times 0.87 \times 1.45 \quad (10)$$

An additional conversion factor, obtained from Table 4, is used to convert the 34 year return interval wind speed calculated with Equation 10 to wind speed at other return intervals of interest.

4.0 RESULTS

4.1 High winds without consideration of relative humidity and temperature

The 50-year return interval 20 ft 3 second gust wind speeds, considering only wind velocity without consideration of relative humidity and temperature, as calculated with this methodology is shown in Figure 3.

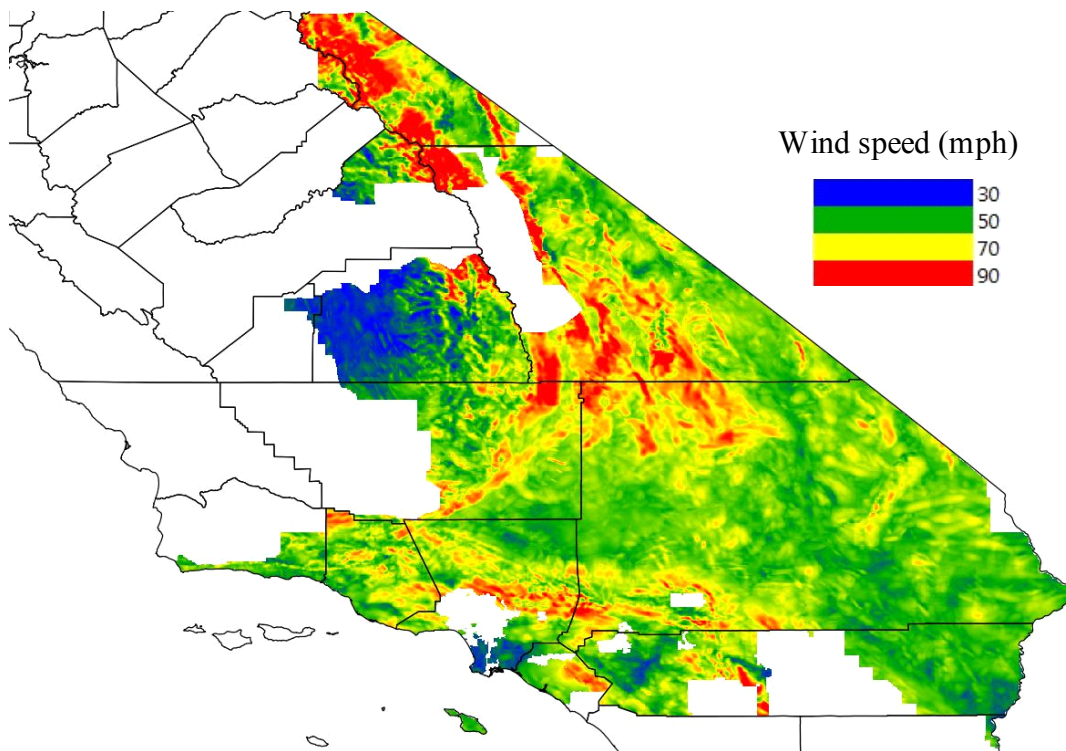


Figure 3. Composite wind loading map for peak wind speeds without consideration of relative humidity and temperature. Velocities are 20 ft wind speeds (3 second gusts) for a 50-year return interval.

4.2 High winds occurring simultaneously with low relative humidity and high temperatures

The 50-year return interval 20 ft 3 second gust wind speeds, for high winds occurring simultaneously with low relative humidity and high temperatures, as calculated with this methodology is shown in Figure 4.

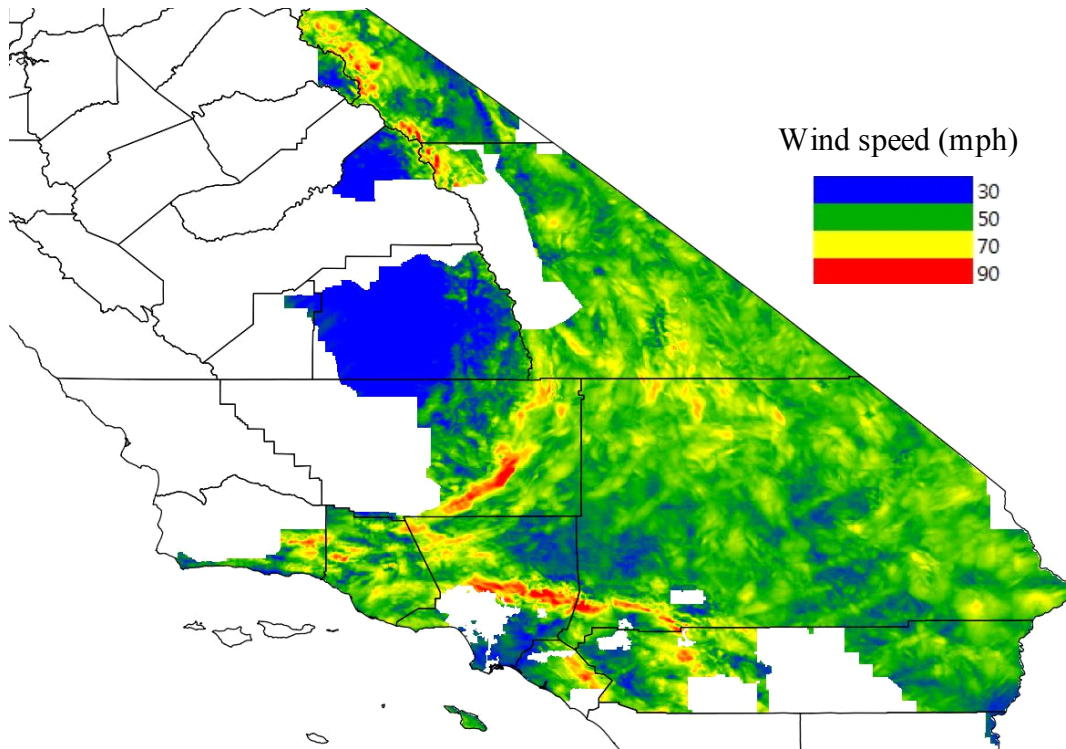


Figure 4. Composite wind loading map for peak wind speeds occurring simultaneously with low relative humidity and high temperatures. Velocities are 20 ft wind speeds (3 second gusts) for a 50-year return interval.

5.0 VALIDATION OF NUMERICAL WEATHER PREDICTION WITH WEATHER STATION DATA

WRF is a widely-used computer model that has been extensively validated. WRF is commonly initialized with the NARR dataset as was done in this work. For these reasons, it is expected that the WRF simulations should provide a satisfactory representation of actual weather conditions in this work. To conform this, the predictive capabilities of WRF in this work were assessed by comparing simulated wind speed/direction, temperature, and relative humidity to hourly surface observations obtained from National Climatic Data Center (NCDC) Dataset (DS) 3505 [6], referred to as Integrated Surface Database (ISD).

DS 3505 contains measurements of dew point, not relative humidity. Therefore, dew point was converted to relative humidity by first calculating the saturation vapor pressure in Pa from temperature in degrees Celsius:

$$P_{ws} = 611.62 \times 10^{\left(\frac{7.5892T_c}{240.71+T_c}\right)} \quad (11)$$

and then calculating relative humidity from dew point (T_d) and ambient temperature as follows:

$$RH = 100 \frac{P_{ws}(T_d)}{P_{ws}(T_\infty)} \quad (12)$$

This facilitated direct comparison of WRF simulation data with surface observations (i.e., weather station measurements) at approximately 100 weather stations within SCE's service territory. Plots were generated to facilitate comparison of measured/modeled quantities (wind speed/direction, air temperature, and relative humidity) at each of these stations. This was done for every event that was simulated. These plots were then manually inspected to assess the level of agreement between observed and modeled quantities. An example of such comparisons is presented in Figure 5. Based on this analysis, it was determined that the WRF simulations demonstrated a satisfactory level of agreement between model calculations and observed quantities, consistent with our previous work in this area.

High Resolution Wind Loading Study
Proprietary and Confidential

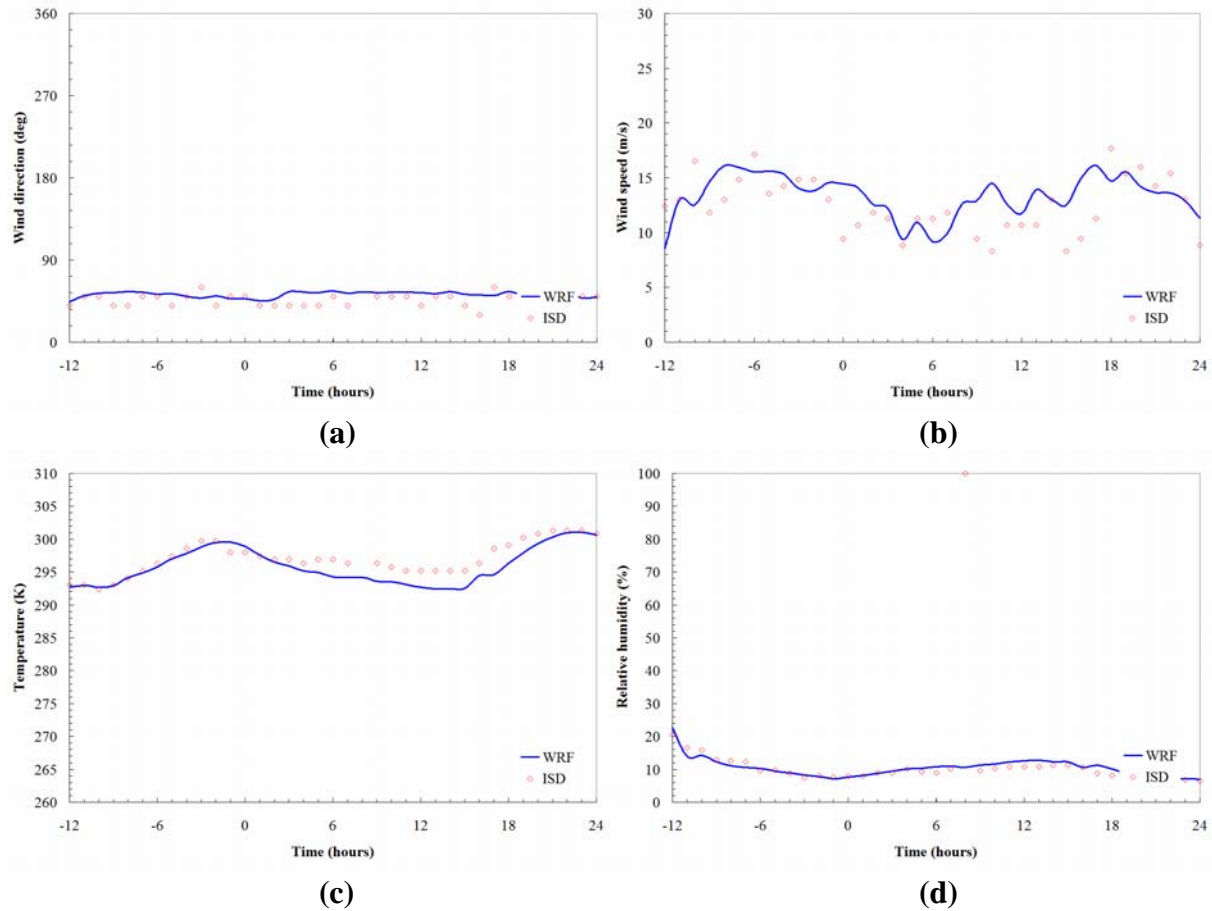


Figure 5. Example of comparison between simulated (WRF) wind speed/direction, air temperature, and relative humidity with surface Integrated Surface Database (ISD) data.

6.0 REFERENCES

- [1] <http://www.wrf-model.org/index.php>
- [2] Fosberg, M.A., "Weather in Wildland Fire Management: The Fire Weather Index," *Conference on Sierra Nevada Meteorology*, American Meteorological Society, pp 1-4 (1978).
- [3] Schroeder, M.J., "Ignition probability," USDA Forest Service. Fort Collins, CO. RMRS unpublished report, 1969.
- [4] Simard, A.J., "The Moisture Content of Forest Fuels – 1. A Review of the Basic Concepts," Canadian Department of Forest and Rural Development, Forest Fire Research Institute, Information Report FF-X-14, Ottawa, Ontario, 47 pp.
- [5] Goodrick, S.L., "Modification of the Fosberg fire weather index to include drought," *International Journal of Wildland Fire* **11**: 205-211 (2002).
- [6] <ftp://ftp.ncdc.noaa.gov/pub/data/noaa/>